BULLETIN OF THE POLISH ACADEMY OF SCIENCES
TECHNICAL SCIENCES, Vol. 61, No. 3, 2013
DOI: 10.2478/bpasts-2013-0069

Particle swarm optimization of an iterative learning controller for the single-phase inverter with sinusoidal output voltage waveform

B. UFNALSKI[1*], L.M. GRZESIAK[1], and K. GAŁKOWSKI[2]

[1] Institute of Control and Industrial Electronics, Warsaw University of Technology, 75 Koszykowa St., 00-662 Warsaw, Poland
[2] Institute of Control and Computation Engineering, University of Zielona Góra, 3b Ogrodowa St., 65-246 Zielona Góra, Poland

Abstract. This paper presents the application of a particle swarm optimization (PSO) to determine iterative learning control (ILC) law gains for an inverter with an LC output filter. Available analytical tuning methods derived for a given type of ILC law are not very straightforward if additional performance requirements of the closed-loop system have to be met. These requirements usually concern the dynamics of a response to a reference signal, the dynamics of a disturbance rejection, the immunity against expected level of system and measurement noise, the robustness to anticipated variations of parameters, etc. An evolutionary optimization approach based on the swarm intelligence is proposed here. It is shown that in the case of the ILC applied to the LC filter, a cost function based on mean squares can produce satisfactory tuning effects. The efficacy of the procedure is illustrated by performing the optimization for various noise levels and various requested dynamics.

Key words: iterative learning control, sine wave inverter, particle swarm optimization.

1. Introduction

Sine wave inverters (also known as true sine wave inverters) have been the essential part of recently heavily developed uninterruptible power supply (UPS) systems and distributed power generation from renewables. A steadily growing demand for more and more accurate control algorithms for these converters is attributed to the need of achieving high quality of the output voltage waveform. There exist various control system synthesis methods for these applications. Majority of them do not exploit repetitiveness of the process under consideration. Standard feedback control, deadbeat control [1], sliding mode control [2] or hysteresis control [3], cannot deliver good performance in the case of a non-linear load as, for instance, a diode rectifier with a capacitor in the DC-link. It should be noted that the considered inverters work in the constant-amplitude constant-frequency (CACF) mode and hence the LC filter control law derivation task can be accomplished by exploiting its repetitive character resulting from the periodic nature of a reference signal and a disturbance. There are several schemes that exploit the process repetitiveness, e.g. solutions with oscillatory terms tuned to the selected frequencies anticipated in the load current [4], solutions derived from the repetitive control theory [5–9], and the iterative learning control theory [10]. Some of these controllers, although designed using different approaches, share many joint features and sometimes are even identical with respect to their topology [5]. The ILC approach is very promising and attractive in applications for various power electronic converters due to a relatively simple and easy for implementation control law. However, frequently when applying to practical situations, after initial error damping its oscillations build-up appears again over the pass-to-pass direction, which feature has to be eliminated. The common way to solve this problem is to apply an additional zero-phase low-pass filter which is aimed to limit the controller learning process to a certain frequency bandwidth. This immunizes the system against periodic disturbances, which otherwise could cause the instability [11]. At the same time, the simple and elegant ILC control law does not imply straightforward analytical tuning methods and linear cost function minimization [12, 13], which task however is known to be non-trivial [14].

Our main goal is to test the possibility of solving these problems by employing evolutionary based optimization methods, with the use of non-parametric performance index, as e.g. the squared control error integral (ISE) or the integral of squared time multiplied control error (ISTE) to eliminate the need for subjective penalty coefficient(s) selection. The only parameters aimed to be selected are the expected noise level and these which govern dynamics of a closed-loop system. Determining the latter should be as simple as possible, e.g. only one time constant of a first-order lag element to be set by the designer. Obviously there is the possibility to extend this research for more sophisticated models and cost functions.

2. Iterative learning control law for LC filter

There is a variety of ILC algorithms, from the simplest, that use only control error from previous and current passes [15], through more complex requiring also full-state information. An example of the latter is presented and analyzed in detail

*e-mail: bartlomiej.ufnalski@ee.pw.edu.pl

in e.g. [11], and was already applied to a single-phase inverter with an LC output filter [10]. In what follows, some key points extracted from [10] are briefly discussed for compactness.

The single-phase inverter depicted in Fig. 1 is considered here as a plant to be controlled. It is important to note that the PSO procedure does not require knowledge of the mathematical model in the state space form as far as a simulational model built in any e.g. drag-and-drop modeling environment like Matlab/Simulink/PLECS is available. To formulate the control law discussed in [10] it is only necessary to identify state variables. For sake of clarity initially the simplified mathematical model of the plant (as in Fig. 2) and resulting controller topology are considered. The LC filter with the non-negligible choke resistance, fed by a pulse width modulated (PWM) converter with negligible dynamics, can be described by the state-space equation of the following form

$$\begin{cases} \dot{\mathbf{x}}(t) = \mathbf{A}_{cont}\mathbf{x}(t) + \mathbf{B}_{cont}u(t) + \mathbf{E}_{cont}i_{load}(t) \\ \mathbf{y}(t) = \mathbf{C}\mathbf{x}(t) \end{cases} \tag{1}$$

with

$$\mathbf{A}_{cont} = \begin{bmatrix} \dfrac{-R_f}{L_f} & \dfrac{-k_i}{L_f k_u} \\ \dfrac{k_u}{C_f k_i} & 0 \end{bmatrix}, \tag{2}$$

$$\mathbf{B}_{cont} = \begin{bmatrix} \dfrac{k_c k_i}{L_f} \\ 0 \end{bmatrix}, \tag{3}$$

$$\mathbf{E}_{cont} = \begin{bmatrix} 0 \\ \dfrac{-k_u}{C_f} \end{bmatrix}, \tag{4}$$

$$\mathbf{C} = \begin{bmatrix} 0 & 1 \end{bmatrix}, \tag{5}$$

$$\mathbf{x} = \begin{bmatrix} i_L^m \\ u_C^m \end{bmatrix}, \tag{6}$$

where R_f, L_f and C_f denote respectively the filter resistance, inductance and capacitance, $u(t)$ is the control signal for the PWM modulator and $i_{load}(t)$ stands for the disturbance (i.e. current drawn by the loads). The superscript m in (6) indicates that the state variables are represented by the measured signals. Physical values of the choke current i_L and the capacitor voltage u_C can be obtained from

$$\begin{cases} i_L^m = k_i i_L \\ u_C^m = k_u u_C \end{cases} \tag{7}$$

where k_i and k_u denote gains introduced by the current an voltage sensors. The PWM converter is assumed here to be an ideal amplifier with the zero delay and the overall gain equal to k_c, which simplification is used only for controller gain determination. The final verification is made for the system with a PWM converter discontinuous model depicted in Fig. 1.

In many applications, a digital implementation is required and most ILC designs assume that this is done by direct digital control, that is, the process dynamics have been sampled by using the zero-order hold discretization method at a uniform rate T_s to obtain a discrete state-space model

$$\begin{cases} \mathbf{x}_k(p+1) = \mathbf{A}\mathbf{x}_k(p) + \mathbf{B}\mathbf{u}_k(p), \quad 0 \le p \le \alpha - 1, \\ \mathbf{y}_k(p) = \mathbf{C}\mathbf{x}_k(p), \end{cases} \tag{8}$$

where

$$\mathbf{A} = e^{\mathbf{A}_{cont}T_s}, \tag{9}$$

$$\mathbf{B} = \int_0^{T_s} e^{\mathbf{A}_{cont}t}\mathbf{B}_{cont}dt \tag{10}$$

and k denotes the finite length (α) trial number. The initial condition for the trial k is taken as the final state of the previous trial.

Note also that the load current representing a disturbance input has been omitted here to simplify an ILC scheme to be solved. However, presence of this disturbance can even destabilize an ILC scheme and further work is required. One of the possible approaches to attenuate a disturbance influence to the process dynamics are based on the H_∞ norm minimization, which is the subject of ongoing work. Also, additional filtering can be used, which can help in avoidance of such negative effects. The simplified description (8) is employed only to derive the control law whereas the influence of the load current is tested in the drag-and-drop model from Fig. 1.

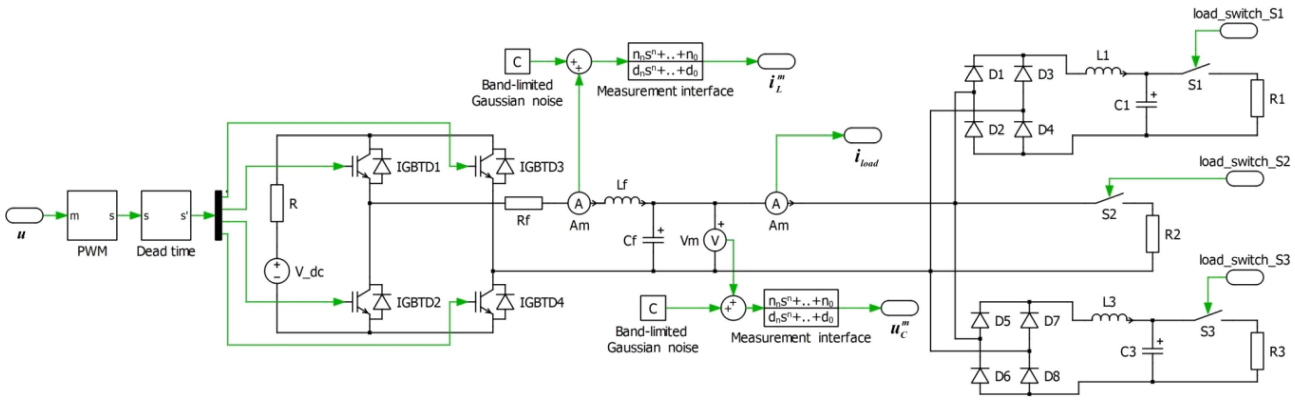

Fig. 1. Schematic diagram of a single-phase inverter with an LC output filter, measurement interface (signal conditioning) and loads

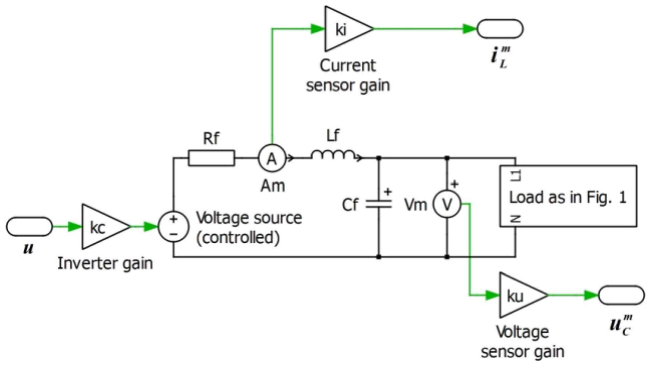

Fig. 2. Simplified model of the single-phase inverter with an LC output filter

A control law under consideration (see [11]) has the form of

$$\Delta u_{k+1}(p) = \mathbf{K}_1 \boldsymbol{\eta}_{k+1}(p+1) + K_2 e_k(p+1), \tag{11}$$

where

$$\Delta u_{k+1}(p) = u_{k+1}(p) - u_k(p) \tag{12}$$

and

$$\boldsymbol{\eta}_{k+1}(p+1) = \mathbf{x}_{k+1}(p) - \mathbf{x}_k(p) = \\ = \begin{bmatrix} i_L^m(k+1,p) \\ u_C^m(k+1,p) \end{bmatrix} - \begin{bmatrix} i_L^m(k,p) \\ u_C^m(k,p) \end{bmatrix}, \tag{13}$$

$$e_k(p+1) = u_C^{ref}(k,p+1) - u_C^m(k,p+1), \tag{14}$$

$$\mathbf{K_1} = \begin{bmatrix} k_{11} & k_{12} \end{bmatrix}, \tag{15}$$

$$K_2 = [k_2] \tag{16}$$

with u_C^{ref} being the reference output voltage multiplied by the measurement gain k_u. This yields the following model

$$\begin{cases} \boldsymbol{\eta}_{k+1}(p+1) = \widehat{\mathbf{A}}\boldsymbol{\eta}_{k+1}(p) + \widehat{\mathbf{B}}_0 e_k(p) \\ e_{k+1}(p) = \widehat{\mathbf{C}}\boldsymbol{\eta}_{k+1}(p) + \widehat{\mathbf{D}}_0 e_k(p) \end{cases}, \tag{17}$$

where

$$\widehat{\mathbf{A}} = \mathbf{A} + \mathbf{B}\mathbf{K}_1, \tag{18}$$

$$\widehat{\mathbf{B}}_0 = \mathbf{B}K_2, \tag{19}$$

$$\widehat{\mathbf{C}} = -\mathbf{C}(\mathbf{A} + \mathbf{B}\mathbf{K}_1), \tag{20}$$

$$\widehat{\mathbf{D}}_\mathbf{0} = \mathbf{1} - \mathbf{C}\mathbf{B}K_2 \tag{21}$$

and hence the closed-loop system dynamics can be investigated using the repetitive process stability theory [11]. Topology of the derived system is sketched schematically in Fig. 3. Note also that the control law (11) has the ability to influence the pass to pass error dynamics only if the first Markov parameter ***CB*** is non-zero (in the SISO case) [13]. In the real system this condition is even stronger because it should be tested under uncertainties of the system parameters and noise. Key parameters of the model are listed in Table 1, where also a first Markov parameter in relation to maximal absolute value of all Markov parameters is included.

Table 1
Key features and parameters of the model

Parameter	Symbol across the paper	Value for filter A (case scenario A)	Value for filter B (case scenario B)
Filter inductance	L_f	600 μH	300 μH
Filter capacitance	C_f	80 μF	160 μF
Resonant frequency	–	726 Hz	726 Hz
Choke resistance	R_f	200 mΩ	100 mΩ
Capacitor series resistance (omitted in the state matrix (2))	–	5 mΩ	10 mΩ
Reference signal frequency	f_{ref}	50 Hz	50 Hz
PWM frequency and controller sample time	$f_{PWM} = \frac{1}{T_s}$	10 kHz	10 kHz
Midpoint in log scale between reference signal frequency and carrier frequency	–	707 Hz	707 Hz
IGBT blanking (dead) time	–	2 μs	2 μs
DC-link voltage	k_c	450 V	450 V
Measurement noise	–	1% and 2% of max. signal value (case scenarios A1 and A2 respectively)	1%
Voltage measurement gain	k_u	1/325 [1/V]	1/325 [1/V]
Current measurement gain	k_i	1/200 [1/A]	1/200 [1/A]
Measurement signal conditioning (measurement interface in Figs. 1 and 4)	–	First order lag element $\tau_m = 50$ μs	First order lag element $\tau_m = 50$ μs
First Markow parameter in relation to the biggest one	–	24%	24%

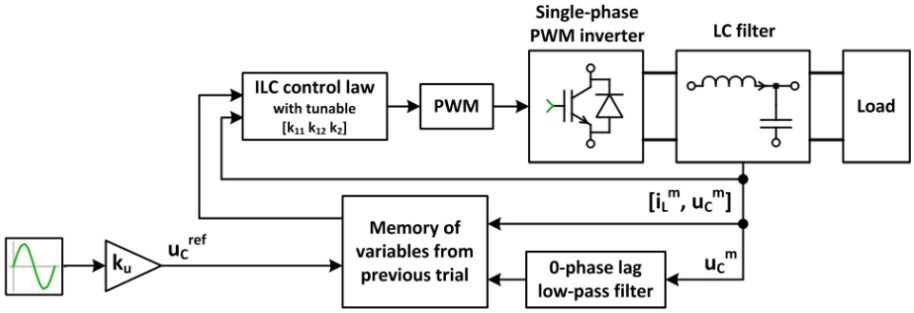

Fig. 3. Schematic diagram of the system

It should be emphasized that the practical implementation of the control law (11), when the mathematical model has been simplified, parameter uncertainty occurs and disturbance are present, requires additional filtering in (14) due to known issue of possible error building-up in long horizon in k-direction [16]. The disturbance input has been intentionally omitted in (8) because its inclusion would complicate significantly the model to be considered. However, it has been verified experimentally that an appropriately designed zero-phase lag low pass filter can stabilize the system for nonlinear periodic disturbances. Thus, in the robust version of (11) the control error is calculated as follows

$$e_k\left(p+1\right) = u_C^{ref}\left(k, p+1\right) - \mathbf{Q}(z)\left(u_C^m\left(k, p+1\right)\right), \quad (22)$$

where a $\mathbf{Q}$-filter spectral characteristic has been set by using the guess and check procedure. Filter coefficients have been calculated using *cheby2* method of the Matlab filter design toolbox and are given in Table 2.

Table 2
Parameters of the zero-phase lag filter

Parameter	Value
Sampling frequency	10 kHz
Passband frequency	500 Hz
Stopband frequency	1000 Hz
Passband ripple	1 dB
Stopband attenuation	20 dB
Design method	*Cheby2* with exact matching of the stopband
Implementation	*filtfilt()* Matlab function
Window width	200 samples
Window center	exactly at $u_C^m(k, p+1)$

A controller gain triple $\{k_{11},\, k_{12},\, k_2\}$ can be designed, see [10], by solving relevant LMI problem. This requires, however, that the system is simplified to the LTI (linear time-invariant) form and all imperfections of measurement interfaces (e.g. noise, delays) are neglected. Also, there is no straightforward way to tune the controller to obtain particular desired dynamics of the closed-loop system. In this paper the whole tuning procedure is redesigned to become a very straightforward optimization task. The controller gain triple $\{k_{11},\, k_{12},\, k_2\}$ aimed to obtain the desired dynamics is found by means of the constricted PSO algorithm with appropriate choice of the cost function. It turns out that a very basic non-parametric performance index like the ISE (integral square error)

$$I_1 = \int_0^{t_{STOP}} \left(u_C^{ref}\left(t\right) - u_C^m\left(t\right)\right)^2 dt \quad (23)$$

with a normalized reference signal

$$u_C^{ref}\left(t\right) = \left(1 - e^{\frac{-t}{\tau_{ref}}}\right) \sin\left(2\pi f_{ref} t\right), \quad (24)$$

where t_{STOP}, τ_{ref} and f_{ref} denote a simulation stop time, a time constant for reference voltage envelope and a reference frequency respectively, is sufficient to produce satisfactory set of controller gains. The advantage of such a performance index is lack of subjective parameters as it is a non-parametric index. To have more influence on the control signal $u(t)$ it is advisable to use a combined performance index, for example,

$$I_2 = \int_0^{t_{STOP}} \left(\left(u_C^{ref}\left(t\right) - u_C^m\left(t\right)\right)^2 + \beta \dot{u}^2\left(t\right)\right) dt, \quad (25)$$

where β is a weighting factor. Note that the index I_1 is a special case of the index I_2 with $\beta = 0$. Such an index introduces a subjective choice of the weighting factor. Both approaches has been tested in this paper. In the discrete form of (25) a scaling factor or a composition with a monotonic function can be introduced to make the result physical interpretation easier. Often the reciprocal of the positive-defined cost function is called a fitness function. These transformations do not influence the behavior of the employed here gradientless optimization method. For the discrete simulations the following fitness function has been chosen:

$$F_{fit} = \left(\frac{\sum_{n=1}^{\frac{t_{STOP}}{T_s}} \left(u_C^{ref}\left(n\right) - u_C^m\left(n\right)\right)^2 + \frac{\beta}{f_{ref}^2}\left(u(n) - u(n-1)\right)^2}{\frac{t_{STOP}}{T_s}} \right)^{-0.5}, \quad (26)$$

where n denotes an integer time index. It should be strongly stressed that the plant model should include plant natural features as nonlinearities, delays, system and measurement noise. Resulting gains are then determined according to the given performance index for certain level of noise and mea-

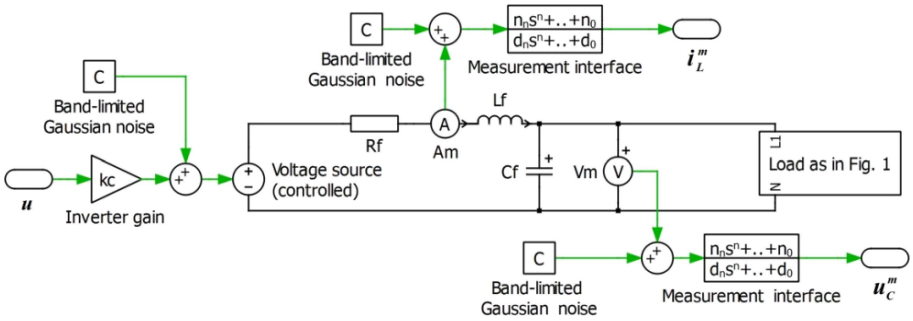

Fig. 4. Schematic diagram of a simplified model of the converter

surement signal conditioning (antialiasing filters, noise cancellation filters). However, this approach has a drawback in that the number of required simulation runs is proportional to the number of particles and to the number of search iterations. Usually it takes several hundred runs to complete the search with a fairy good result. That is why we have decided to approximate the pulse width modulated converter with an ideal gain. The effect of the system noise has been modeled by adding a 0.5% noise to the control signal as in Fig. 4. This significantly reduces computational burden of the method used. The original model with PWM requires at least 1 μs simulation step size to give trustworthy numerical results whereas its simplified version can be run with the frequency of the control system, i.e. 10 kHz. The t_{STOP} time in (26) also has to be carefully chosen, as too small value results in poor reliability of the assessment of the performance, whereas too big slows down the optimization process. Taking into account the dynamics of the discussed system (Table 1) together with a number of the test loads (Table 3), $t_{STOP} = 10$ s turns out to be reasonable.

3. Particle swarm optimization (PSO)

Evolutionary algorithms are often used in multidimensional and multiobjective nonlinear optimization problems. Numerous examples include mechanical design [17] and signal processing [18] tasks. In particular, PSO is a stochastic optimization algorithm. An optimizer is initialized with a set called swarm of random candidate solutions called particles. Particles travel through the space of the problem solutions and are rated in each iteration according to the selected objective function. Their movements are influenced by the global best solution and the particle's best solution found so far. Note that a search path for each particle is not deterministic. There is a random factor that modifies the strength of individual and social behaviour for each particle in each iteration as the fixed coefficients c_1 and c_2 of the velocity update rule (27) are multiplied by a random number. Thus, the core of the basic algorithm, under the assumption that the global best solution is the only information shared among particles, can be written as [19]:

$$\begin{aligned}\mathbf{v}_i\left(n+1\right) = c_1\mathbf{v}_i\left(n\right) + c_2\text{rand}()\left(\mathbf{x}_i^{pbest} - \mathbf{x}_i\left(n\right)\right) \\ + c_3\text{rand}()\left(\mathbf{x}^{gbest} - \mathbf{x}_i\left(n\right)\right),\end{aligned} \tag{27}$$

$$\mathbf{x}_i\left(n+1\right) = \mathbf{x}_i\left(n\right) + \mathbf{v}_i\left(n+1\right), \tag{28}$$

where the following notations were used:
i – particle identification number,
n – iteration number,
$\mathbf{v}_i$ – speed of the i-th particle,
$\mathbf{x}_i$ – position of the i-th particle,
$\mathbf{x}_i^{pbest}$ – best solution proposed so far by i-th particle (*pbest*),
$\mathbf{x}^{gbest}$ – best solution found so far by the swarm (*gbest*),
c_1 – explorative factor (inertia weight),
c_2 – individuality factor,
c_3 – sociality factor,
rand() – uniformly distributed between 0 and 1 random number.

If the rule (27) manifests unsatisfactory convergence speed or limited ability to find the optimum or acceptable suboptimum, numerous modifications are described in the literature, see e.g. [20]. However, it has been tested that the original PSO scheme is effective for the ILC application considered here. Hence, no modifications regarding information flow have been made. Constant factors present in the rule are set according to so called constricted PSO algorithm [21]:

$$\begin{aligned}\mathbf{v}_i\left(n+1\right) = \chi\left[\mathbf{v}_i\left(n\right) + \frac{\varphi}{2}\text{rand}()\left(\mathbf{x}_i^{pbest} - \mathbf{x}_i\left(n\right)\right)\right. \\ \left. + \frac{\varphi}{2}\text{rand}()\left(\mathbf{x}^{gbest} - \mathbf{x}_i\left(n\right)\right)\right],\end{aligned} \tag{29}$$

where φ is chosen to be equal to 4.1 and the resulting χ is then 0.73 as in [21].

For the discussed ILC control law design, each particle is a vector

$$\mathbf{x}_i = \left[\begin{array}{ccc} k_{11} & k_{12} & k_2 \end{array}\right] \tag{30}$$

of candidate settings for the controller gains. All search directions are assumed to be unconstrained. It is common practice to set limits (walls for the particles) if clear physical boundaries are identifiable. Here no additional analysis of (11) is assumed, e.g. regarding acceptable signs of the gains. A numerical model of the system can be run with any set of real valued gains. Unstable solutions have lower fitness than the stable ones and they do not attract particles. A schematic diagram of the control system connected to the PSO optimizer is shown in Fig. 5.

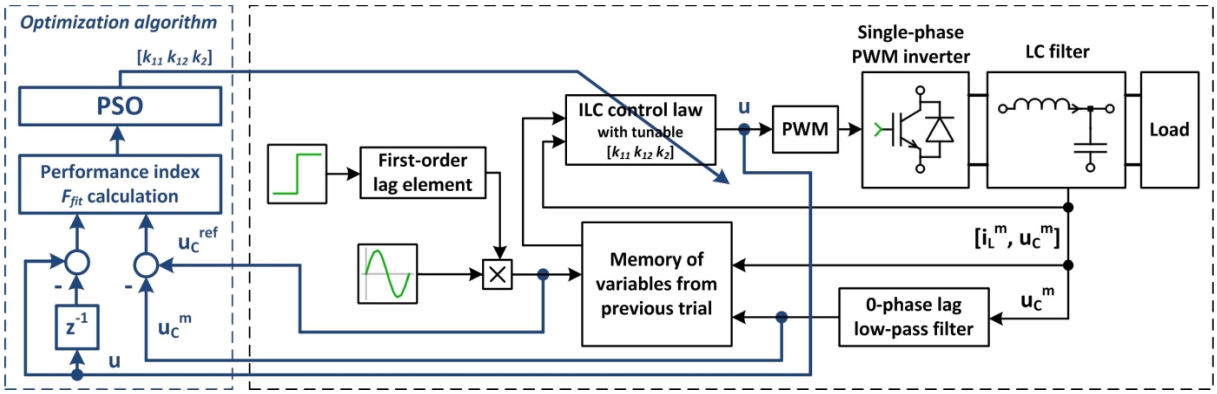

Fig. 5. Schematic diagram of the system connected to the PSO optimizer

4. Numerical experiment

The detailed numerical model of the power electronic converter has been prepared in Matlab/Simulink/PLECS environment. The PWM controlled inverter is one of the sources of a system noise. To accommodate this phenomenon in the linear model of the inverter a white noise is added to the control signal (Fig. 4). Peak-to-peak white noise levels stated in Table 1 are given in reference to the peak-to-peak value of a measured variable. A practical peak-to-peak value of the white noise is calculated using the crest factor equal to 4 (this threshold is not crossed around 98% of the time). This reflects a common practice to the Gaussian noise peak-to-peak value approximation, where rare peaks are omitted [22].

The electrical part of the system together with the modulator are implemented in the PLECS subsystem, where the rest of the model is implemented in Simulink mainly by means of S-Function Builder. All models are simulated using fixed step solver at 10 kHz for linear approximation of the inverter and at 1MHz for discontinuous description of the inverter (i.e. with the transistor switches and the pulse width modulator). The test scenario includes switching (see switches S1, S2 and S3 in Fig. 1) between different loads summarized in Table 3.

Table 3
Test loads

Load no. 1	Load no. 2	Load no. 3
Diode rectifier	Linear resistive load	Diode rectifier
L_1 = 250μH		L_3 = 500μH
C_1 = 3mF		C_3 = 3mF
R_1 = 20Ω	R_2 = 5Ω	R_3 = 7Ω
Approx. P_1= 5kW	Approx. P_2= 10kW	Approx. P_3= 15kW
S1 is on from 0.5s to 3s	S2 is on from 3s to 5s	S3 is on from 5s

The PSO function is coded in the M-file and calls the model of the converter to calculate value of the fitness function. Several performance indices have been taken into account including IAE, ISE and IGSE. The fitness function (26) has been selected by trial and error method, which leads to the satisfactory behavior of the system and lack of subjective penalty factors (if the derivative term is skipped). However, it is advisable to set $\beta > 0$ to get the possibility to influence the dynamics of the control signal, which is important in a real noisy system case. Key features of PSO used here are listed in Table 4.

Table 4
Key parameters of the swarm

Particle	$[k_{11}$ k_{12} $k_2]$ controller gains
Swarm size	27 particles
Number of iterations	max. 45
Boundary conditions	None
Algorithm modifications	None (standard constricted PSO)

No assumptions are made regarding a search space when the swarm is initialized. However, to make an optimization process reasonable in terms of the wall clock time, the starting positions of the particles should form a cloud that embraces regions of possible good solutions. Hence, input and output signals of the controller have been normalized to the range of -1 to 1. Then, the swarm has been initialized to uniformly cover a cube with edge length equal to 1000 centered at (0,0,0) and it has been tested that the vast majority of solutions returned during the first 10 iterations are unstable. Thereafter, the cube has been reduced to $100\times100\times100$ and still the majority of solutions during the first 10 iterations are unstable. The starting distribution of the particles for all following optimization experiments is bounded to 10x10x10 cubic space. Although the search space is unbounded, in none of the cases indicated in Table 1 particles tend to move outside this cube. Usually, no more than 30 iterations are required to obtain a satisfactory implementable solution. The swarm is kept alive until 45-th iteration just for better assessment of its convergence. The color of the particle refers to its best solution found so far. Specific values are provided in Table 5.

Table 5
Colors according to particle's best solution

Fitness function F_{fit} value threshold	Color of a particle
>20	magenta
>10	blue
>5	cyan
>2	green
below all thresholds	red

In all mentioned here scenarios the swarm converges towards zero speed and optimization results are repeatable. This suggests that the problem is well-conditioned. Several other LC filters, noise levels and load types have been also tested and results of all of them confirm effectiveness of the tuning procedure. Robustness of the control system has been also verified by testing several hypothetical load currents drawn by controlled current sources. This includes triangular and square currents. The gains found in the scenarios A1, A2, B1, B2 and B3 are collated in Table 6. The reference signal for all experiments is taken as in (24) with $\tau_{ref} = 0.5$ s (A1, A2, B1, B3) or $\tau_{ref} = 0.3$ s (B2). A change of τ_{ref} clearly influences the dynamics of the resulting closed-loop system. It is also to note that the modification of a reference signal amplitude, which is not present in the target system of Fig. 3, becomes essential during the optimization procedure illustrated in Fig. 5. This enables to specify dynamics of the system by setting desired rise time for the output voltage envelope. To illustrate this, the envelopes of the output voltage waveform in B1 and B2 are shown in Figs. 6 and 7 respectively. These results have been obtained using the reference signal not modified by the first-order lag element (Fig. 3). This means that the rise time of the envelope is shaped solely by the controller dynamics and not by modification of the reference signal. It is also possible to influence the dynamics of the system by changing in (26) the penalty factor β. For comparison purposes the MSE (mean square error) evolution for the scenarios B1 and B3 has been shown in Figs. 8 and 9 respectively. The derivative term in the experiment B3

Table 6
Controller gains optimized according to the F_{fit} performance index

Case scenario	k_2 (related to control error)	k_{11} (related to change in choke current)	k_{12} (related to change in capacitor voltage)
A1: 1% noise L_f = 600 μH C_f = 80 μF R_f = 200 mΩ τ_{ref} = 0.5 s $\beta = 10^{-4}$	0.325	−3.87	−6.74
A2: 2% noise L_f = 600 μH C_f = 80 μF R_f = 200 mΩ τ_{ref} = 0.5 s $\beta = 10^{-4}$	0.267	−3.30	−5.22
B1: 1% noise L_f = 300 μH C_f = 160 μF R_f = 100 mΩ τ_{ref} = 0.5 s $\beta = 10^{-4}$	0.262	−1.93	−5.93
B2 as in B1 yet different envelope dynamics $\tau_{ref} = 0.3$ s	0.326	−1.38	−3.88
B3 as in B1 but different penalty factor $\beta = 10^{-3}$	0.211	−1.64	−4.23

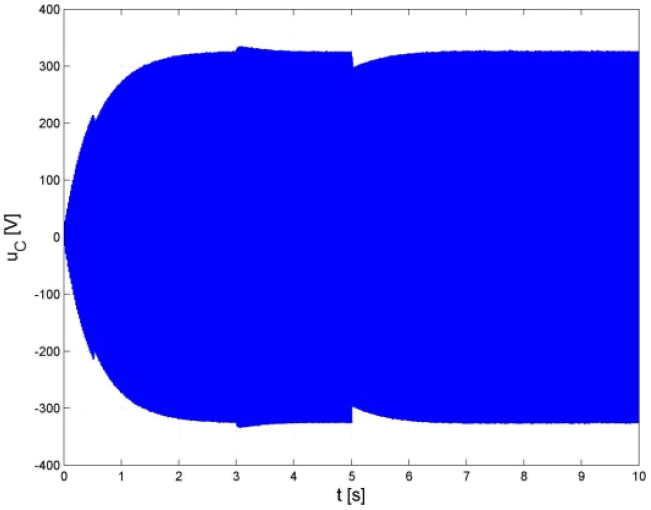

Fig. 6. The envelope of the output voltage waveform if optimized using $\tau_{ref} = 0.5$ s (case B1)

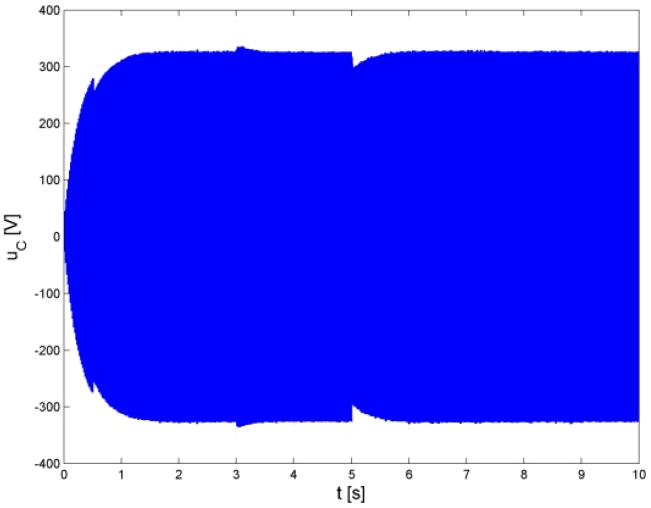

Fig. 7. The envelope of the output voltage waveform if optimized using $\tau_{ref} = 0.3$ s (case B2)

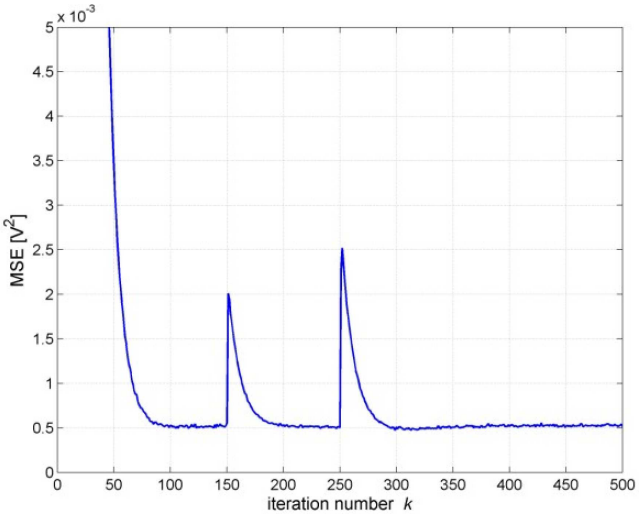

Fig. 8. The evolution of the mean squared error in system optimized using a relatively small penalty factor for control signal dynamics (case B1, $\beta = 10^{-4}$)

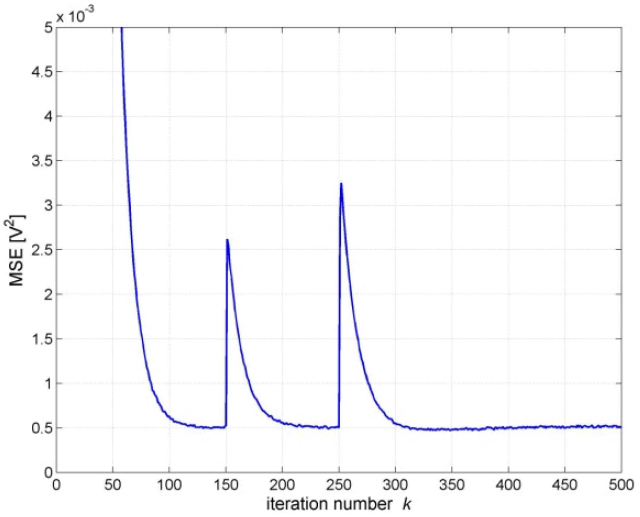

Fig. 9. The evolution of the mean squared error in system optimized using a moderate penalty factor for control signal dynamics (case B3, $\beta = 10^{-3}$)

contributes in approximately 50% to the sum of squares in (26) for *gbest* solution. It is clear that τ_{ref} as well as β can be used to shape the response. The former affects mainly a tracking dynamics whereas the latter influences a disturbance rejection dynamics. However, these effects are convoluted and one cannot shape them independently.

For illustrative purposes some graphs obtained during the B3 test are also presented. The position of the swarm after 1, 10, 25 and 45 iterations is depicted in Figs. 10 to 13. The variances of all controller gains versus number of the iteration are presented in Figs. 14, 15 and 16. The evolution of variances is a reliable indicator of the swarm behavior. If the variance crosses a specific threshold resulting from measurement noise there is no justification for further search and the procedure should be stopped. Performance of the system with gains found by the PSO is then investigated in the model with PWM converter (as shown in Fig. 1). The plots of the measured (thus corrupted by the noise) output voltage and the control signal along with the disturbance current are shown in Figs. 17, 18 and 19. The MSE in Fig. 9 comes from the same experiment and shows that the learning occurs and after the error increase caused by a change of the load it goes down again over the consecutive trials. The instantaneous control error is depicted in Fig. 20. This error is huge at the start of the system due to zero initial conditions for the LC filter. The output voltage quality under load 3 (see Table 3) at 10 s, i.e. 5 s after switching this load on, is presented in Fig. 21. The choke current ripples are as in Fig. 22. For comparison purposes the open-loop performance is illustrated in Fig. 23.

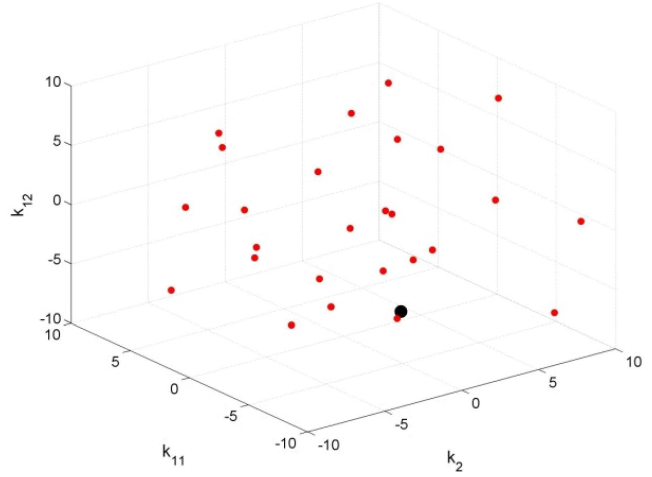

Fig. 10. Initial particles position: *gbest* = [−2.51, −7.42, 1.80], *fitness* = 11.1

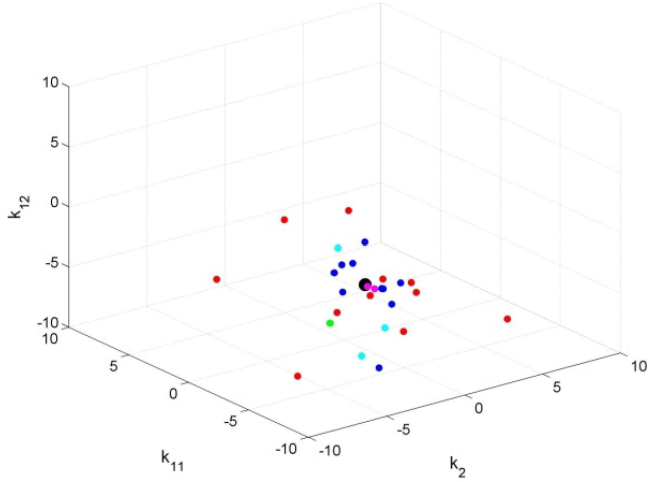

Fig. 11. Particles position after 10 iterations (case B3): *gbest* = [−1.38, −4.83, 0.254], *fitness* = 33.4

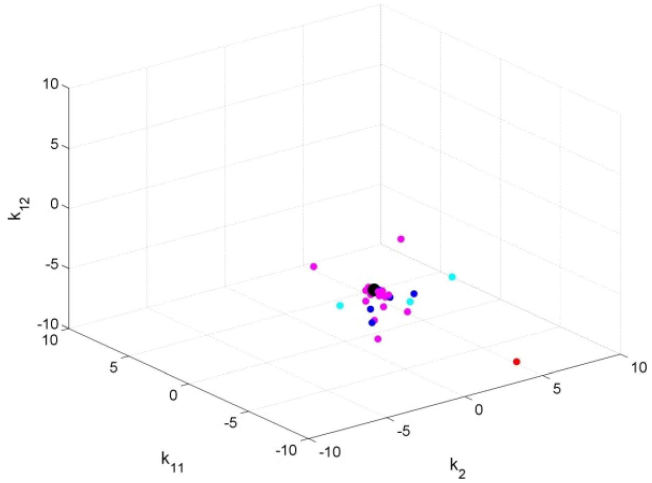

Fig. 12. Particles position after 25 iterations (case B3): *gbest* = [−2.13, −4.80, 0.087], *fitness* = 38.5

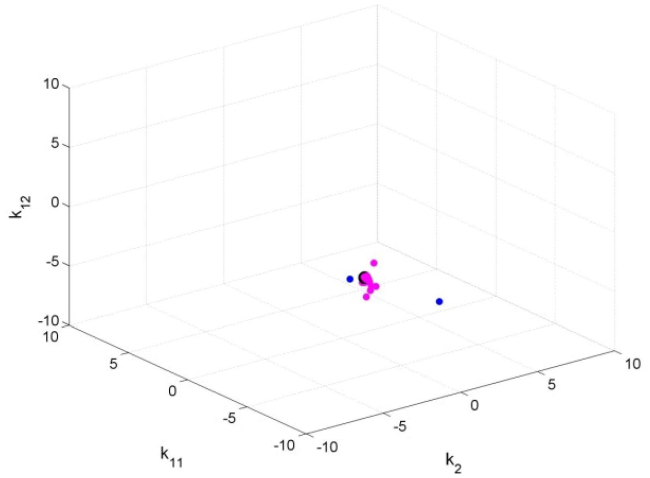

Fig. 13. Particles position after 45 iterations (case B3): *gbest* = $[-1.64, -4.23, 0.211]$, *fitness* = 39.7

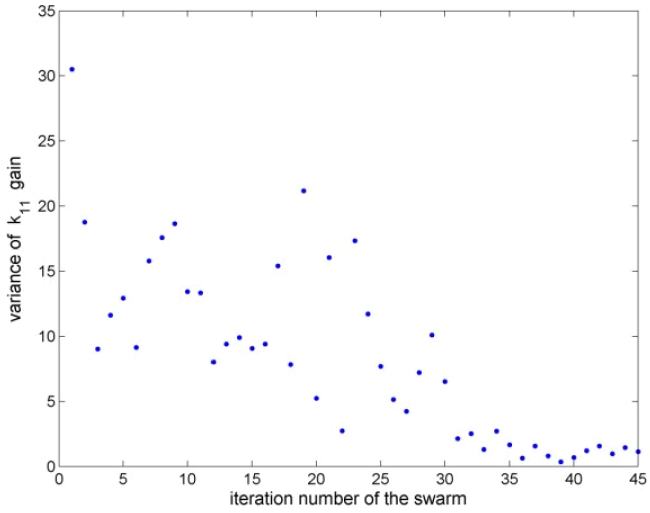

Fig. 14. The variance of the controller k_{11} gain versus optimization iteration (case B3)

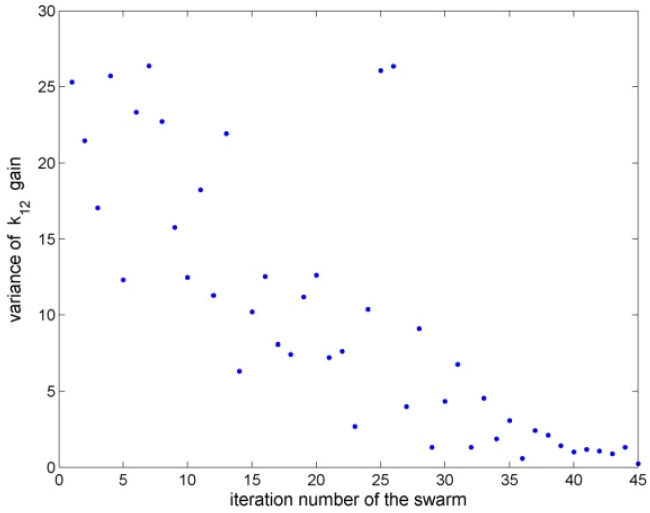

Fig. 15. The variance of the controller k_{12} gain versus optimization iteration (case B3)

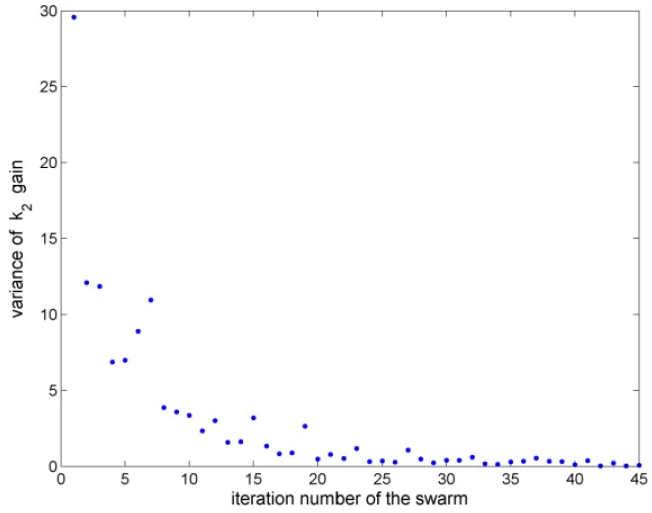

Fig. 16. The variance of the controller k_2 gain versus optimization iteration (case B3)

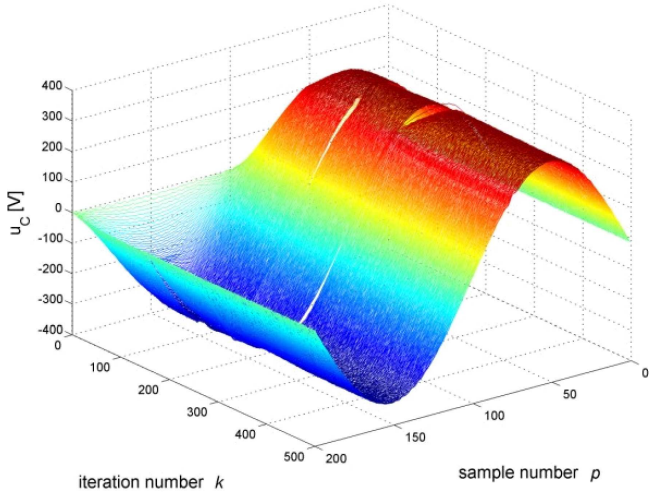

Fig. 17. The evolution of the output voltage over consecutive passes (case B3)

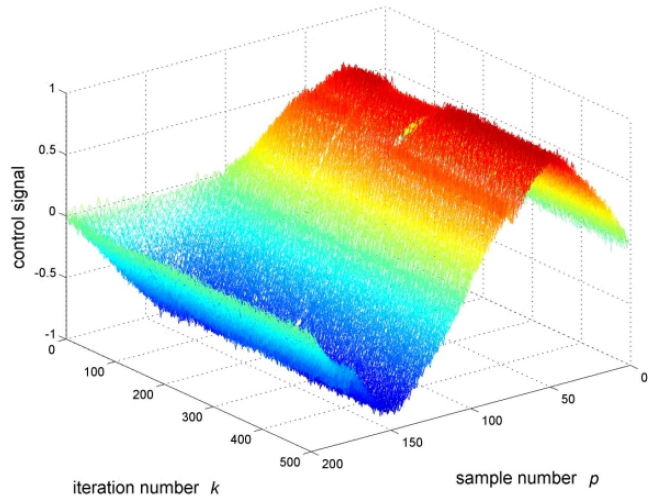

Fig. 18. The evolution of the control signal u over consecutive passes (case B3)

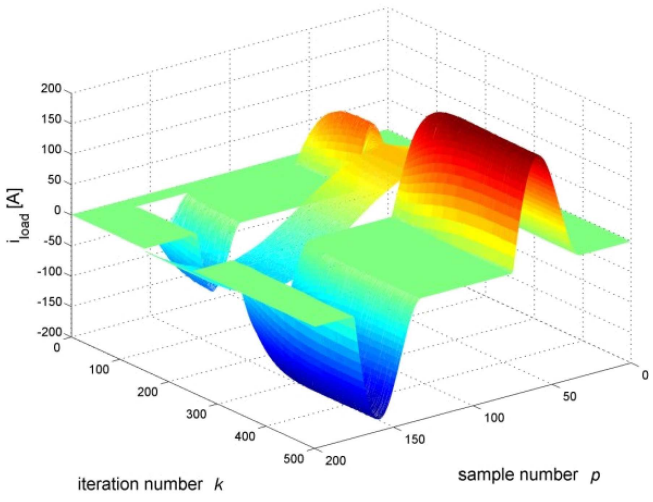

Fig. 19. The shape of the test load current (case B3)

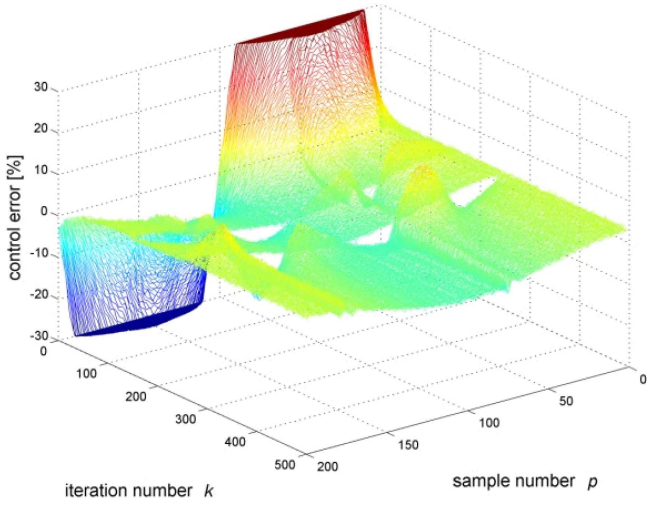

Fig. 20. The evolution of the control error over consecutive passes (case B3)

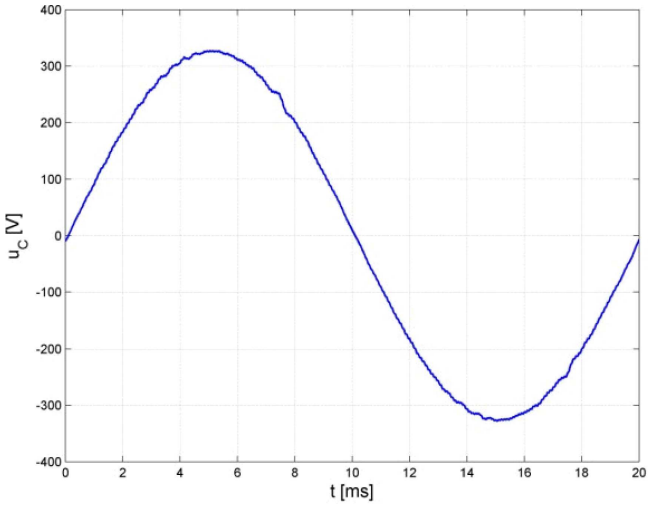

Fig. 21. The shape of the output voltage 5s from switching the diode rectifier on (load no. 3, case B3)

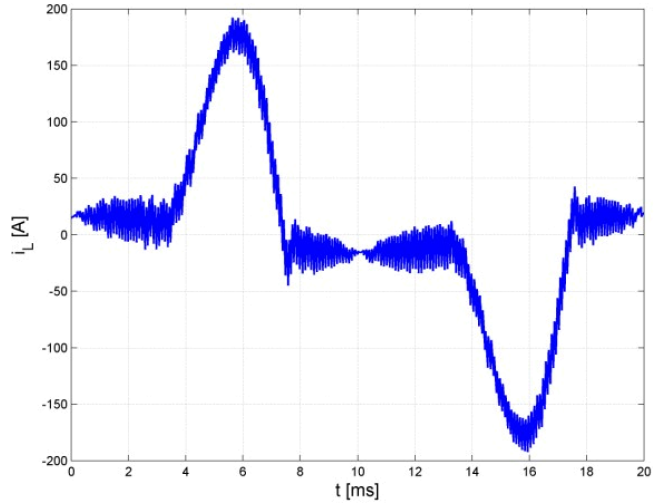

Fig. 22. The shape of the choke current 5s from switching the diode rectifier (load no. 3, case B3)

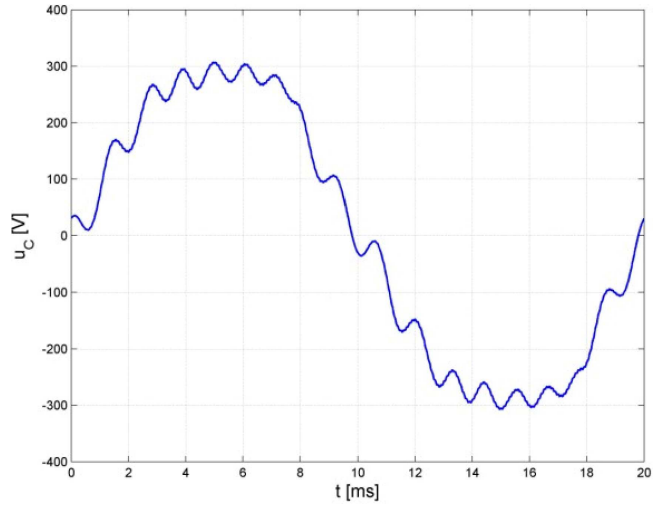

Fig. 23. The shape of the output voltage if load no. 3 is on and the controller is off (open-loop operation)

5. Stability issues

Due to that there exist disturbance and parameter uncertainties affected by unpredictable and variable loads the analytical proof of the stability for the obtained closed-loop system is very difficult or even impossible to perform. It should be noted that the LMI approach used in [10] can be helpful for producing such a proof but only for the case with no disturbance (load current) which, as shown before, is in fact an intrinsic part of the considered system and any, even the linear, load can cause instability. One of the approaches to obey these problems relies on applying robust ILC schemes, e.g. with filtering action as in (22). It has been already identified that the periodic nonlinear load current can cause instability if no zero-phase lag filtering is applied to the output voltage measurement signal (as in (14)). One can also test gains found by means of the PSO analytically by checking relevant LMI problem or graphically by drawing the Nyquist plot [23]

but this only proves that the linear system without the disturbance is stable. Hence, the numerical simulation with the fairy accurate model that includes, inter alia, the PWM, the modulator dead-time, the measurement noise, the 0-phase lag filter and the disturbance is currently the only way to identify overall stability issues. It has been tested that for all sets of gains found by the use of the PSO algorithm (with fitness assessed in the window of 10s) the system with nonlinear loads turns out to be stable in long horizon and the control signal does not display any abnormalities even after tens of minutes.

6. Conclusions

The PSO procedure has been employed to tune the ILC gains for the true sine wave converter. It has been shown that the LMI approach commonly used in the class of ILC schemes can be replaced with a very straightforward optimization procedure. Moreover, several limitations entailed by the LMI approach (i.e. noiseless LTI description) are easy to evade if evolutionary approach is chosen. Evaluation of the controller during the optimization procedure can be performed using a nonlinear model of the plant with all filters needed in a practical realization. The system can be tested during the optimization process against specific disturbances, e.g. specific nonlinear loads. Typical imperfections and parasitic effects including noise, delays, parameters variations can be taken into account. Obtained results indicate that the problem is well-conditioned and the population based stochastic optimization process is fully repeatable and insensitive, in terms of its convergence, to reasonable levels of system and measurement noise. Numerical experiments assuming a nonlinear model of the inverter manifest a stable operation over a long time horizon. A physical experimental converter is currently under the development.

Acknowledgements. The research work has been partially supported by the Electrical Drive Division of the Warsaw University of Technology statutory funds for 2012/2013 and by the National Science Centre in Poland, the grant No. 2011/01/B/ST7/00475.

REFERENCES

[1] K.P. Gokhale, A. Kawamura, and R.G. Hoft, "Dead beat microprocessor control of PWM inverter for sinusoidal output waveform synthesis", *IEEE Trans. on Industry Applications* 23 (5), 901–910 (1987).

[2] M. Carpita and M. Marchesoni, "Experimental study of a power conditioning system using sliding mode control", *IEEE Trans. on Power Electronics* 11 (5), 731–742 (1996).

[3] A. Kawamura and R. Hoft, "Instantaneous feedback controlled PWM inverter with adaptive hysteresis", *IEEE Trans. on Industry Applications* 20 (4), 769–775 (1984).

[4] A. Kaszewski, L.M. Grzesiak, and B. Ufnalski, "Multi-oscillatory LQR for a three-phase four-wire inverter with L3nC output filter", *Proc. IEEE Industrial Electronics Society 38th Annual Conf.* IECON, 3449–3455 (2012).

[5] G. Escobar, A.A. Valdez, J. Leyva-Ramos, and P. Mattavelli, "Repetitive-based controller for a UPS inverter to compensate unbalance and harmonic distortion", *IEEE Trans. on Industrial Electronics* 54 (1), 504–510 (2007).

[6] K. Zhou, D. Wang, B. Zhang, and Y. Wang, "Plug-in dual-mode-structure repetitive controller for CVCF PWM inverters", *IEEE Trans. on Industrial Electronics* 56 (3), 784–791 (2009).

[7] B. Zhang, D. Wang, K. Zhou, and Y. Wang, "Linear phase lead compensation repetitive control of a CVCF PWM inverter", *IEEE Trans. on Industrial Electronics* 55 (4), 1595–1602 (2008).

[8] K. Zhou, K.-S. Low, D. Wang, F.-L. Luo, B. Zhang, and Y. Wang, "Zero-phase odd-harmonic repetitive controller for a single-phase PWM inverter", *IEEE Trans. on Power Electronics* 21 (1), 193–201 (2006).

[9] Y. Ye, K. Zhou, B. Zhang, D. Wang, and J. Wang, "High-performance repetitive control of PWM DC-AC converters with real-time phase-lead FIR filter", *IEEE Trans. on Circuits and Systems II: Express Briefs* 53 (8), 768–772 (2006).

[10] R. Kulawinek, K. Galkowski, L. Grzesiak, and A. Kummert, "Iterative learning control method for a single-phase inverter with sinusoidal output voltage", *Proc. IEEE Industrial Electronics Society 37th Annual Conf.* IECON, 1402–1407 (2011).

[11] L. Hladowski, K. Galkowski, Z. Cai, E. Rogers, C.T. Freeman, and P.L. Lewin, "Experimentally supported 2D systems based iterative learning control law design for error convergence and performance", *Control Engineering Practice* 18 (4), 339–348 (2010).

[12] E. Rogers, K. Galkowski, and D.H. Owens, *Control Systems Theory and Applications for Linear Repetitive Processes (Lecture Notes in Control and Information Sciences 349)*, Springer, Berlin, 2007.

[13] L. Hladowski, K. Galkowski, E. Rogers, Z. Cai, C.T. Freeman, and P.L. Lewin, "Iterative learning control for discrete linear systems with zero Markov parameters using repetitive process stability theory", *Proc. IEEE International Symp. on Intelligent Control* (ISIC), 400–405 (2011).

[14] K.L. Moore, E. Rogers, and K. Galkowski, "Modeling, analysis, and design of repetitive processes and iterative learning control systems", *Workshop IEEE Multi-Conf. on Systems and Control*, http://control.mines.edu/netrob09/MSC_DRP_Workshop.html) (2012).

[15] D.A. Bristow, M. Tharayil, and A.G. Alleyne, "A survey of iterative learning control", *IEEE Control Systems* 26 (3), 96–114 (2006).

[16] L. Hladowski, Z. Cai, K. Galkowski, E. Rogers, C.T. Freeman, and P.L. Lewin, "Using 2D systems theory to design output signal based iterative learning control laws with experimental verification", *Proc. 47th IEEE Conf. on Decision and Control* (CDC), 3026–3031 (2008).

[17] M. Szczepanik and T. Burczyński, "Swarm optimization of stiffeners locations in 2-D structures", *Bull. Pol. Ac.: Tech.* 60 (2), 241–246 (2012).

[18] A. Słowik, "Application of evolutionary algorithm to design minimal phase digital filters with non-standard amplitude characteristics and finite bit word length", *Bull. Pol. Ac.: Tech.* 59 (2), 125–135 (2011).

[19] J. Kennedy and R. Eberhart, "Particle swarm optimization", *Proc. IEEE Int. Conf. on Neural Networks* 4, 1942–1948 (1995).

[20] B. Ufnalski and L.M. Grzesiak, "Particle swarm optimization of artificial-neural-network-based on-line trained speed controller for battery electric vehicle", *Bull. Pol. Ac.: Tech.* 60 (3), 661–667 (2012).

[21] R.C. Eberhart and Y. Shi, "Comparing inertia weights and constriction factors in particle swarm optimization", *Proc. Congress on Evolutionary Computation* 1, 84–88 (2000).

[22] *The Axon Guide. A Guide to Electrophysiology & Biophysics Laboratory Techniques*, 3rd ed., MDS Analytical Technologies, 2008.

[23] W. Paszke, P. Rapisarda, E. Rogers, and M. Steinbuch, "Dissipative stability theory for linear repetitive processes with application in iterative learning control", *Proc. Symposium on Learning Control IEEE Conf. on Decision and Control* 1, CD-ROM (2009).